DINAME 2019 - Proceedings of the XVIII International Symposium on Dynamic Problems of Mechanics,
M.A. Savi, T.G. Ritto and W.M. Bessa (Editors), ABCM, Buzios, RJ, Brazil, March 10th to 15th, 2019

Flexible piezoelectric cantilever under Vortex-Induced Vibrations

Letícia Siqueira Madi[1], **Celso Pupo Pesce**[2] **and Guilherme Rosa Franzini**[3]

Offshore Mechanics Laboratory, Escola Politécnica, University of São Paulo, São Paulo, Brazil.

[1]leticia.madi@usp.br; [2]ceppesce@usp.br; [3]gfranzini@usp.br

Abstract: This paper proposes a reduced order model (ROM) for a piezoelectric energy harvesting device fed by Vortex-induced vibrations (VIV). The system is composed of a cantilevered flexible polymeric cylinder molded over a beam. The beam is covered by thin layers of piezoelectric material, connected in series to a resistive element. The harvester is considered to exhibit geometric linear behaviour, linear elastic effects of the piezoelectric material and linear coupling to a power harvesting circuit. The hydrodynamic loads are introduced by wake-oscillators models. Numeric simulations are performed for analysing the cantilever displacements and electrical power harvested.

Keywords: Vortex-induced vibrations, wake-oscillator models, energy harvesting, piezoelectric effects

INTRODUCTION

The search for alternative energy sources is a prominent subject and a recent technological demand, with a special focus on clean energy generation. In addition, the growth in the use of portable electronic devices demands new technologies regarding batteries and energy storage. In this context, vibration-based energy harvesting has become a topic in evidence. Energy harvesting from vortex-induced vibrations phenomena is an interesting approach, since VIV is a fluid-structure interaction that leads to self-excited and self-limited oscillations. As an example, Bernitsas et al. (2006) presents the concept of VIVACE (Vortex-Induced Vibration Aquatic Clean Energy), a device based on a series of cylinders in tandem arrangement that uses electromagnetic transducers to convert structural kinetic energy into electricity. See more recent studies on VIVACE in Liu and Bernitsas (2015), Ding et al. (2016) and Sun et al. (2017).

Flexible piezoelectric devices have already a long history of successful research concerning actuation and sensing technology for smart material systems. In the context of vibratory energy harvesting, piezoelectric materials are gaining attention to its use on energy generation. This kind of harvester is particularly useful for reduced power demands for electronic devices in the micro and milliWatt scale, such as self-reliant electrical micro systems like remote sensors.

Considering this scenario, this paper proposes a simplified reduced order model as an initial approach for studying a cantilevered piezoelectric harvester under VIV, coupling mechanical and electrical responses. The hydrodynamic loads due to the fluid-structure interactions are modeled using the wake-oscillator concept, which employs van der Pol equations to represent the wake dynamics, as in Ogink and Metrikine (2010). After presenting the reduced order model formulation in the next section, some preliminary results are shown, produced trough numerical simulations and a brief discussion is given.

MATHEMATICAL MODEL

Inspired by the experimental work by Defensor Fo (2018) (see also Defensor Fo. et al (2018)), who studied the dual resonance phenomenon of flexible cantilivers under VIV, the harvester is composed of a cantilevered flexible polymeric cylinder of length L and diameter D, molded over a flat bar constituted by a metallic substract placed between two piezoelectric material layers, which are connected in series to a resistive element R. The system and the axis definition are represented in Fig. 1. For this preliminary model, displacements are allowed only on the yz vertical plane, perpendicular to the income flow. The 3D problem will be addressed in a further paper.

Cantilever model

In this preliminary study, it is considered that the beam vibrates according to the first mode only. This is common in VIV of cantilevered cylinders; see Pesce and Fujarra (2000). This simplifying asumption is taken even being the authors aware that resonance in higher bending modes would be much more beneficial in energy harvesting. In fact, as VIV is a resonant phenomenon, the higher the frequency excited, the larger will be the power extracted. Moreover, VIV is a self-controlled phenomenon, with typical amplitudes of order of one diameter. Therefore, the higher the mode the larger are dynamic curvatures. So a double gain is obtained by exciting higher modes. In the present case, the cantilever displacements can be given by a function $\Psi(z,t)$, which can be separated on the vibration mode $\phi(z)$, and the modal amplitude generalized coordinate $Y(t)$.

$$\Psi(z,t) = \phi(z)Y(t) \tag{1}$$

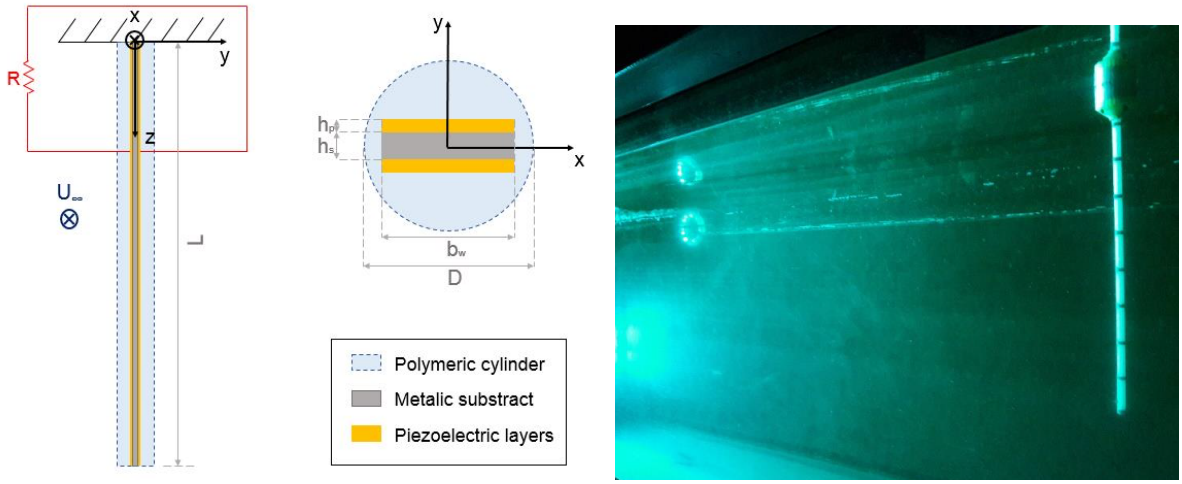

Figure 1 – Schematic representation of the cantilever model and experimental mounting of a flexible cantilever in a water channel (Defensor Fo., 2018).

As well known, the function for a single linear vibration mode of a clamped-free beam is shown in Eq. 2, where Λ and σ are dimensionless parameters related to the the vibration mode; see, e.g., Blevins (2001).

$$\phi(z) = \cosh\left(\frac{\Lambda}{L}z\right) - \cos\left(\frac{\Lambda}{L}z\right) - \sigma\left[\sinh\left(\frac{\Lambda}{L}z\right) - \sin\left(\frac{\Lambda}{L}z\right)\right] \tag{2}$$

The cross section properties are given by Eqs. 3 to 6. Dimensions b_w, h_s and h_p represent, respectively, the beam width, the substract and the piezoelectric layer thicknesses.

$$\mathscr{M}^{(s)} = 0 \tag{3}$$

$$I^{(s)} = \frac{b_w h_s^3}{12} \tag{4}$$

$$\mathscr{M}^{(p)} = \pm\frac{b_w h_p h_s}{2}\left(1+\frac{h_p}{h_s}\right) \tag{5}$$

$$I^{(p)} = \frac{b_w h_p^3}{12} + \frac{b_w h_p h_s^2}{4}\left[1+\frac{h_p}{h_s}+\left(\frac{h_p}{h_s}\right)^2\right] \tag{6}$$

The kinetic energy of the system is given by

$$T = \frac{1}{2}(m_c+m_s+m_p+m_a)\int_0^L \left[\dot{\Psi}(z,t)\right]^2 \mathrm{d}z = \frac{1}{2}\mu\dot{Y}^2(t)\int_0^L [\phi(z)]^2\,\mathrm{d}z \tag{7}$$

On the other hand, for small amplitude oscillations, the harvester is considered to exhibit a linear geometric behaviour, being $\varepsilon_{zz} = -y\Psi$" the expression for the beam strain. Notice that this compatibility equation refers to the Bernoulli-Euler beam model. The bending-strain potential energy of the system, without the piezoelectric layers is, therefore:

$$U_c = \frac{1}{2}(EI)_{eq}\int_0^L \left[\Psi''(z,t)\right]^2 \mathrm{d}z = \frac{1}{2}(EI)_{eq}Y^2(t)\int_0^L \left[\phi''(z)\right]^2 \mathrm{d}z \tag{8}$$

In order to give the whole formulation a more compact form, following Mineto (2013), some modal fuction integrals are defined as follows.

$$\int_0^L [\phi(z)]^2\,\mathrm{d}z = \Phi_{20} \tag{9}$$

$$\int_0^L \phi''(z)\mathrm{d}z = \Phi_{12} \tag{10}$$

$$\int_0^L \left[\phi''(z)\right]^2 \mathrm{d}z = \Phi_{22} \tag{11}$$

The modeling of the piezoelectric circuit considers linear elastic effects and coupling of the electric circuit. Equations 12 and 13 are the piezoelectric material expressions for the mechanical stress T_{zz} and electrical displacement D_y ; see

Erturk and Inman (2011).

$$T_{zz} = \bar{c}^E_{zz}\varepsilon_{zz} - \bar{e}_{yz}E_y \tag{12}$$

$$D_y = \bar{e}_{yz}\varepsilon_{zz} + \bar{\varepsilon}^s_{yy}E_y \tag{13}$$

The piezoelectric material constants $\bar{c}^E_{zz}$ and $\bar{e}_{yz}$ are the elastic and electroelastic tensor components. The elastic tensor values are as measured in a zero electric field. The electric permittivity at zero strain is $\bar{\varepsilon}^s_{yy}$. The electric field E_y can be written as a function of the electric tension in the form $E_y = \pm\dfrac{V(t)}{h_p}$. The potential energy for one layer of the piezoelectric material is then given by equation 14

$$U_p = \frac{1}{2}\int_{V_p}\left(T_{zz}\varepsilon_{zz} - D_y E_y\right)\mathrm{d}V_p \tag{14}$$

The piezoelectric layers are connected in series, thus the potential energy for both layers is given by equation 15.

$$U = I_p\bar{c}^E_{zz}Y^2\Phi_{22} - \frac{\bar{e}_{yz}}{4h_p}V\mathscr{M}_p\Phi_{12} - \frac{V^2}{4h_p}\bar{\varepsilon}^s_{yy}b_wL \tag{15}$$

The external excitation is modelled by a distributed force $f_y(z,t)$ along the entire beam. The virtual work related to this non-conservative force is given by

$$\delta w^{n.c.} = \delta\int_0^L f_y(z,t)\Psi(z,t)\mathrm{d}z = \delta Y\int_0^L f_y(z,t)\phi(z)\mathrm{d}z \tag{16}$$

Therefore, from equation 16, the definition of generalized force gives that

$$Q_y = \int_0^L f_y(z,t)\phi(z)\mathrm{d}z \tag{17}$$

The equations of motion for the system are then derived from the corresponding Lagrange's equations as described in Mineto (2013). The final dimensional equations for the modal coordinate $Y(t)$ and the electrical potential $V(t)$ are given by Eqs. 18 and 19, being $\mathscr{M}^{(p)}$ referent to the superior piezoelectric layer.

$$\mu\Phi_{20}\ddot{Y} + c_f\Phi_{20}\dot{Y} + \left((EI)_{eq} + 2I\bar{c}^E_{zz}\right)\Phi_{22}Y - \frac{\bar{e}_{yz}}{h_p}\mathscr{M}^{(p)}\Phi_{12}V = \int_0^L f_y(z,t)\phi(z)\mathrm{d}z \tag{18}$$

$$\frac{\bar{\varepsilon}^S_{yy}}{2h_p}b_wL\dot{V} + \frac{\bar{e}_{yz}}{h_p}\mathscr{M}^{(p)}\Phi_{12}\dot{Y} + \frac{V}{R} = 0 \tag{19}$$

The total linear mass of the system is $\mu = (m_c + m_s + m_p + m_a)$, where m_c, m_s and m_p are the linear mass of the cylinder, the substract and the piezoelectric laminates. The parameter m_a is the first mode added mass that takes the value $m_a = 1.17m_d$, where m_d is the displaced fluid mass; see Pesce and Fujarra (2000) or Salles and Pesce (2018).

The distributed load $f_y(z,t)$ comes from the fluid-structure interaction. This hydrodynamic parameter will be modeled through an wake-oscillator approach, described in the next subsection.

Wake-oscillator model

Regarding the vortex-induced vibrations phenomenon, this paper adapts the models for rigid cylinders mounted on elastic bases presented in Ogink and Metrikine (2010) and Franzini and Bunzel (2018). Following these models, the hydrodynamic loads are composed of drag and lift forces. A fictitious wake variable q representing the vortex-wake dynamics, is assumed to be related to the lift coefficient C_L in the form of $C_L = \dfrac{\hat{C}^0_L}{\hat{q}}q$. The coefficient $\hat{C}^0_L$ is the amplitude of the lift coefficient observed in experiments with fixed cylinders subjected to perpendicular and steady flow. In such class of wake oscillator models, a van der Pol's equation is usually adopted for representing the fluid dynamics, and an acceleration coupling scheme is used for the solid-fluid interaction; see, e.g., the earlier works by Hartlen and Currie (1970) and by Iwan and Blevins (1974). Equation 20 represents the wake dynamics, where ω_s is the vortex-shedding frequency, and ε and A are parameters to be experimentally calibrated. The adaptation for the flexible cylinder model is made by assuming that the wake variable q is a function of time and of the modal coordinate of the cantilever, as in Eq. 21; see Orsino et al. (2018a, 2018b). This is based on the fact that, during the lock-in phenomenon, the structural response regulates the wake dynamics, by controlling the vortex shedding frequency.

$$\ddot{q} + \varepsilon\omega_s\left(q^2 - 1\right)\dot{q} + \omega_s^2 q = \frac{A}{D}\ddot{\Psi} \tag{20}$$

$$q(z,t) = \phi(z)\bar{q}(t) \tag{21}$$

The force caused by vortex-shedding is then considered as a distributed load described at each section z as a function of the drag and lift coefficients, the free-stream velocity U_∞ and the flow velocity relative to the cylinder, U. The fluid density is ρ.

$$f_y(z,t) = \frac{1}{2}\rho D\left(\frac{U}{U_\infty}\right)^2\left(C_L\frac{U_\infty}{U} - C_D\frac{\Psi}{U}\right) \tag{22}$$

The coefficient $\hat{q} = 2$ is the amplitude of the limit-cycle periodic homogeneous solution. The parameter $C_D = \bar{C}_D^0$ is the mean drag coefficient observed for a fixed cylinder.

Dimensionless equations

Length variables z and Y are made dimensionless by the cylinder total length and diameter, and the time variable by the first mode natural frequency in still water ω_n. The electric voltage V is written in terms of a reference value V_0. The reduced velocity U_r and the Strouhal parameter St are also defined as follows.

$$y = \frac{Y}{D} \qquad \tau = \omega_n t \qquad \xi = \frac{z}{L} \qquad v = \frac{V}{V_0}; V_0 = \frac{m_d\omega_n^2 D}{e_{xx}} \qquad St = \frac{\omega_s D}{2\pi U_\infty} \qquad U_r = \frac{U_\infty 2\pi}{\omega_n D}$$

Equations 1 and 21 are now written as Eqs. 23 and 24. Following Orsino et al. (2018a, 2018b), an auxiliary function $p(\xi,\tau)$ is introduced, defined as in Eq. 25.

$$\Psi(\xi,\tau) = \phi(\xi)Dy(\tau) \tag{23}$$

$$q(\xi,\tau) = \phi(\xi)\bar{q}(\tau) \tag{24}$$

$$\dot{p}(\xi,\tau) = \left(q^2-1\right)\dot{q} = \phi(\xi)\dot{\bar{p}}(\tau) \tag{25}$$

The dimensionless equations for the modal amplitude, the electric tension and the wake variable may then be deduced in the form

$$\ddot{y} + 2\zeta\dot{y} + ky - \chi_1 v = Q\left(\frac{\hat{C}_L^0}{\hat{q}}\bar{q} - \bar{C}_D^0\frac{2\pi\dot{y}}{U_r}\right)\int_0^1\sqrt{1+\left(\frac{2\pi\dot{y}}{U_r}\phi(\xi)\right)^2}\,\phi^2(\xi)\mathrm{d}\xi \tag{26}$$

$$\dot{v} + \chi_2\dot{y} + \chi_3 v = 0 \tag{27}$$

$$\ddot{\bar{q}} + \varepsilon StU_r\dot{\bar{p}} + (StU_r)\,\bar{q} = A\ddot{y} \tag{28}$$

where the dimensionless parameters are defined as follows.

$$\zeta = \frac{c_f}{2\mu\omega_n} \quad k = \frac{\left((EI)_{eq} + 2I\bar{c}_{zz}^E\right)\bar{\Phi}_{22}}{\mu\omega_n^2 L^4\bar{\Phi}_{20}} \quad \chi_1 = \frac{\bar{e}_{yz}\mathscr{M}^{(p)}V_0\bar{\Phi}_{21}}{h_p\mu DL^2\bar{\Phi}_{22}} \quad \chi_2 = \frac{2\bar{e}_{yz}D\mathscr{M}^{(p)}\bar{\Phi}_{21}}{b_w\bar{\varepsilon}_{yy}^S L\omega_n V_0} \quad \chi_3 = \frac{2h_p}{\bar{\varepsilon}_{yy}^S\omega_n R} \quad Q = \frac{m_d U_r^2}{\mu 2\pi^3\bar{\Phi}_{20}}$$

$$\int_0^1\left[\phi(\xi)\right]^2\mathrm{d}\xi = \bar{\Phi}_{20} \qquad \int_0^1\phi''(\xi)\mathrm{d}\xi = \bar{\Phi}_{12} \qquad \int_0^1\left[\phi''(\xi)\right]^2\mathrm{d}\xi = \bar{\Phi}_{22}$$

NUMERIC SIMULATIONS

Equations 26 to 28 were numerically integrated using Mathematica® NDSolve function. Time step for the results is $\Delta\tau = 0.01$ and maximum dimensionless time $\tau_{max} = 2000$. The reduced velocities vary from 0 to 15, and $\Delta Ur = 0.15$. The only non-trivial initial condition is $q(0) = 0.01$. Steady-state responses are considered only for $\tau > \tau_{max}/2$. Amplitude measures of y and v for each reduced velocity are considered $A_y = rms \times \sqrt{2}$, where the *rms* are calculated for the steady state series, being implict that a quasi-sinusoidal motion is expected.

The mode of vibration function in Eq. 2 uses the first mode values for parameters Λ and σ as in Blevins (2001). The cylinder mass, diameter, length and bending stiffness parameters are adopted as in Defensor Fo.(2018), just as the metallic substract parameters. The piezoelectric material elastic and electroelastic constants are considered as in Mineto (2013). The adopted values are summed up in Tab. 1. The parameters of the wake-oscillator model are the ones presented in Ogink and Metrikine (2010), in Tab. 2.

The simulations performed aim at analysing the cantilever displacements on the first mode of vibration, as much as the electrical power harvested from them.

RESULTS AND DISCUSSION

Two cases were simulated: pure VIV, without considering the effects of the piezoelectric layers; and VIV coupled with the piezoelectric system. For better understanding of the phenomena, illustrative time series are plotted. Figure 2

Table 1 – Values adopted for the parameters in simulations.

Parameter	Adopted value
Λ	1.87510407
σ	0.734095514
L	1 m
D	0,1 m
b_w	0,004 m
h_s	0,001 m
h_p	$h_s/10$
m_p	0,006 kg/m
m_c	34,55 kg/m
m_s	0,27 kg/m
$\bar{c}^E_{zz}$	60,6 GPa
$\bar{e}_{yz}$	16,6 C/m^2
$\bar{\varepsilon}^S_{yy}$	30 nF
R	100 kΩ

Table 2 – Parameters of the wake-oscillator model.

ε	0,05	$Ur < 6,5$
A	4	
ε	0,7	$Ur > 6,5$
A	12	
$\tilde{C}^0_L$	0,3842	
C^0_D	1,1856	$0 < Ur < 15$
St	0,1932	

shows that the amplitudes of the modal displacement and the wake variable increase with time, reaching a steady state response. In Fig. 3 are ploted time series for three different reduced velocities: at the initial amplitude response branch, at the lock-in peak and at the lower branch. It is possible to see how the frequencies increase with the reduced velocities, locking-on with the natural frequency in the resonance region, while the amplitudes reach a peak and decrease. Figure 4 shows the peak of the amplitude response at each reduced velocity simulated. A comparison between amplitude responses for VIV without and with piezoelectric effects is also presented.

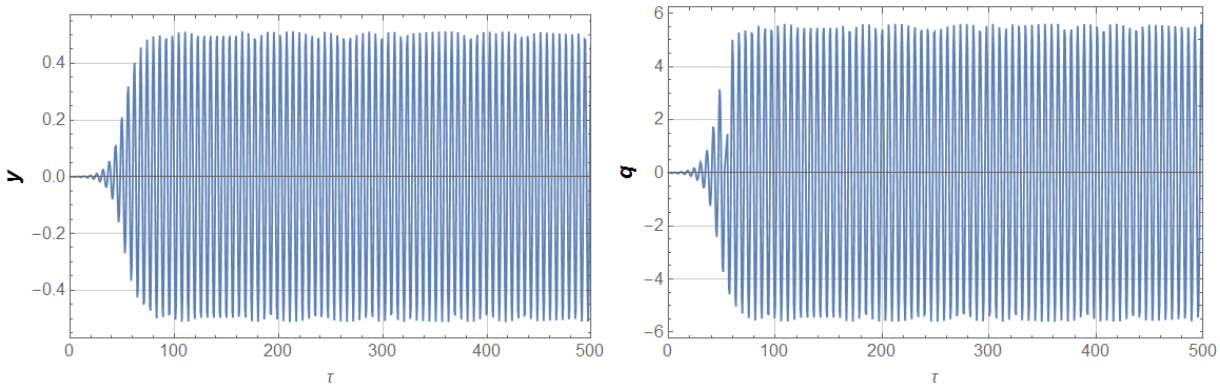

Figure 2 – Time series of the modal displacements and wake variable, at $\mathbf{U_r = 5.5}$

For the system simulated without considering the piezoelectric layers, an upper and lower branches of amplitude response are identified, and the maximum amplitude for coordinate $y(\tau)$ is around 0.55. When the system includes the piezoelectric circuit, for the adopted parameters, the amplitude values decrease, reaching a peak of 0.50. The constant χ_1 is of order 10^{-6}, with small effects on the system when compared to the other parameters of equation 26, causing this small reduction.

Figure 5 represents the maximum electric tension generated from the system as a function of reduced velocity. This graphic shows that, for the lower branch, the electric tension decreases more slowly than the reduction of the displace-

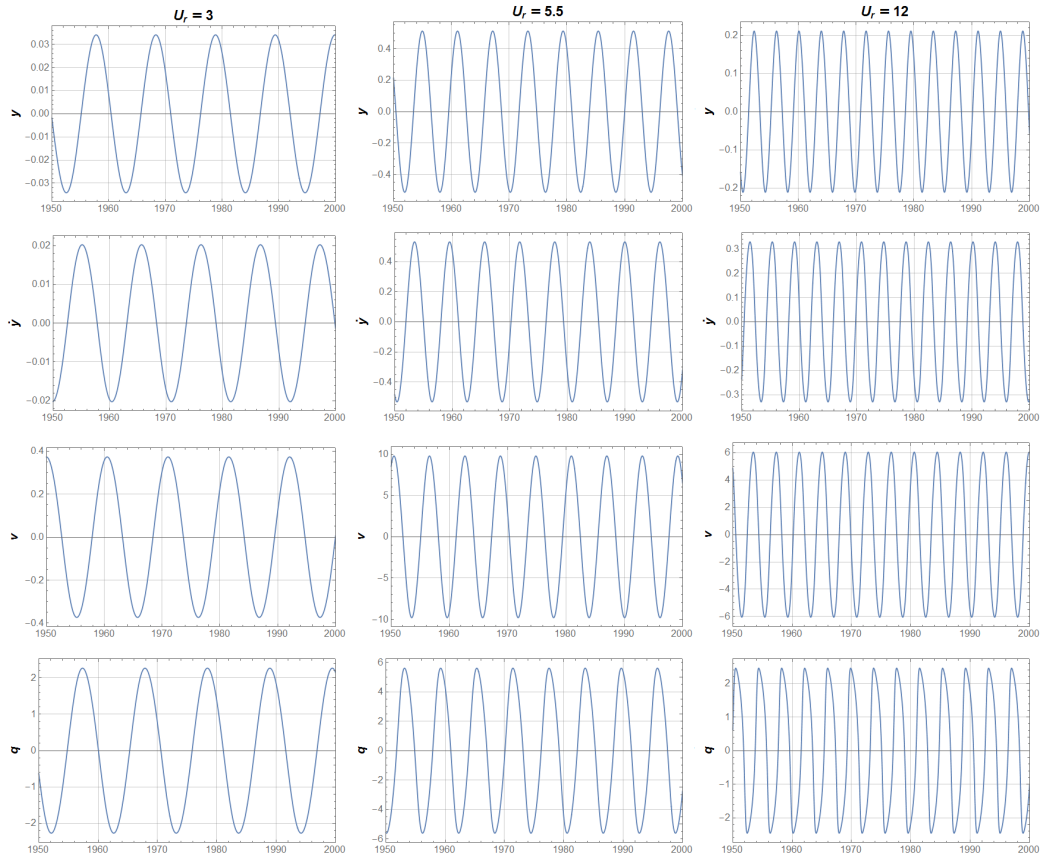

Figure 3 – Time series for different reduced velocities, at already reached steady state regimes.

ments. This is because oscillation frequency increases.

For this case study, the maximum electric power harvested from the system can be estimated as in Eq. 29.

$$P = \frac{V_{max}^2}{R} = \frac{(0,025\,V)^2}{100k\Omega} \approx 62.5nW \tag{29}$$

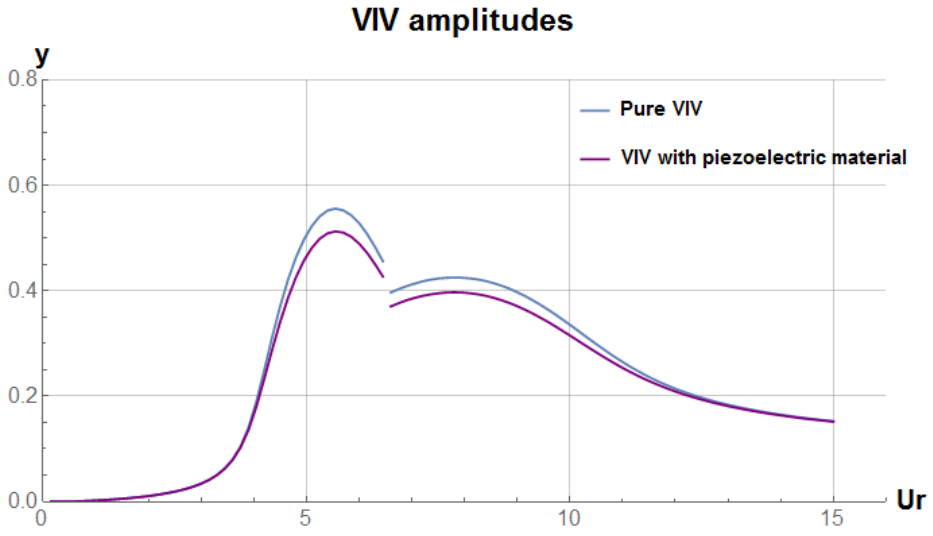

Figure 4 – Response branches for VIV with and without piezoelectric coupling

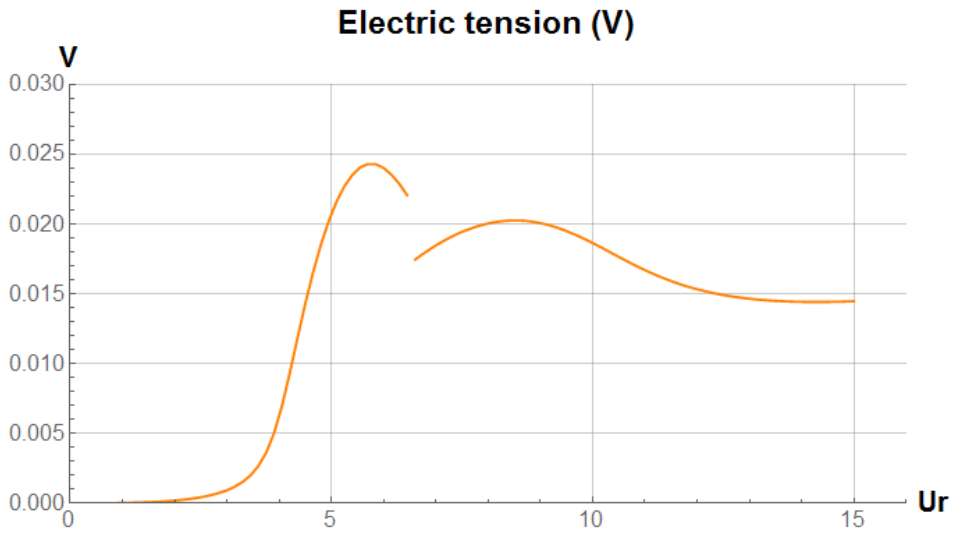

Figure 5 – Amplitude of electric tension generated.

CONCLUDING REMARKS

A model was developed as a first approach for the coupling of the mechanical and electrical responses for a bimorph piezoeletric substrat material over a cantilever undergoing VIV. For this 2D unimodal case, the maximum amplitude of the dimensionless modal coordinate at lock-in peak is 0.55 diameters for pure VIV. When considered the piezoelectric coupling, the peek is reduced in approximately 10%, and the maximum power harvested is $62.5nW$.

The representativeness of the modeling in 2D must be further investigated, since the dual resonance that takes place between in-line and cross-wise oscillations in 3D dynamics can cause important effects; see e.g. Defensor (2018). The model can be extended considering higher vibrating modes, at which a significant increase in power harvested might be expected. The parameters of the wake-oscillator, calibrated for the rigid cylinder mounted on an elastic base, must also be verified for the flexible cylinder.

ACKNOWLEDGMENTS

The first author acknowledges PPGEN - Graduate Program in Naval and Ocean Engineering, social demand CAPES MSc scholarship, and the Technological Research Institute of São Paulo State IPT for the 'Novos Talentos' program. Dr. Renato Orsino, MSc Wagner Defensor Fo and Eng. Guilherme Vernizzi are gratefully acknowledged, for their kind suggestions and help. The second and third authors are grateful to the Brazilian National Research Council (CNPq) for the research grants n. 308990/2014-5 and 310595/2015-0.

REFERENCES

Bernitsas,M.M.; Raghavan, K.; Ben-Simon, Y.; Garcia, E. M. H. VIVACE (vortex induced vibration aquatic clean energy): A new concept in generation of clean and renewable energy from fluid flow. Journal of Offshore Mechanics and Arctic Engineering, 2008.

Blevins, R. D. Formulas for Natural Frequency and Mode Shape. Krieger Pub Co, 2001. ISBN 1-57524-184-6.

Defensor Fo., W.A., Investigação experimental de vibrações induzidas por escoamento em cilindros flexíveis com rigidez ortotrópica. MSc Dissertation (in Portuguese), Escola Politécnica, USP, 2018.

Ding, L.; Zhang, L.; Bernitsas, M.M.; Chang, C. Numerical simulation and experimental validation for energy harvesting of single-cylinder VIVACE converter with passive turbulence control. Renewable Energy, Elsevier BV, v. 85, p. 1246-1259, jan 2016.

Erturk, A.; Inman, D. J., Piezoeletric energy harvesting. John Wiley & Sons, 2011.

Franzini, G. R.; Bunzel, L. O. A numerical investigation on piezoelectric energy harvesting from vortex-induced vibrations with one and two degrees of freedom. Journal of Fluids and Structures, Elsevier BV, v. 77, p. 196-212, feb 2018.

Hartlen, R.T.; Currie, I.G.: Lift Oscillator Model of Vortex-Induced Vibration, Proceedings of the ASCE, 1970.

Iwan, W. D.; Blevins, R. D. A model for Vortex-Induced Oscillation of Structures. Journal of Applied Mechanics, v.41, p. 581-586, 1974.

Liu, J.; Bernitsas, M.M. Envelope of Power Harvested by a Single-Cylinder VIVACE Converter. Volume 9: Ocean Renewable Energy, ASME, 2015.

Mineto, A. T. Geração de energia a partir da vibração estrutural de dispositivos piezelétricos não-lineares. PhD Thesis (in Portuguese) - São Carlos Engineering School of University of São Paulo, 2013.

Ogink, R.;Metrikine, A. A wake oscillator with frequency dependent coupling for the modeling of vortex-induced vibration. Journal of Sound and Vibration, Elsevier BV, v. 329, n. 26, p. 5452-5473, dec 2010.

Orsino, R.M.M.; Pesce, C.P.; Franzini, G.R. A 3D non-linear reduced order model for a cantilevered pipe conveying fluid under VIV. Proceedings of 9th International Symposium on Fluid-Structure Interactions, Flow-Sound Interactions, Flow-Induced Vibration and Noise, Toronto, Ontario, Canada, 2018a.

Orsino, R.M.M.; Pesce, C.P.; Franzini, G.R. Cantilevered pipe ejecting fluid under VIV: Non-linear reduced order modeling and analysis. 2018b (Submitted)

Pesce, C.P., Fujarra, A.L.C., 2000, Vortex-Induced Vibrations and Jumping Phenomenon: An experimental investigation with a clamped flexible cylinder in water, Int. J of Offshore and Polar Engineering, Vol.10 (1), pp. 26-33.

Salles R., Pesce C.P. (2018) Experimental Assessments of the Added Mass of Flexible Cylinders in Water: The Role of Modal Shape Representation. In: Fleury A., Rade D., Kurka P. (eds) Proceedings of DINAME 2017. DINAME 2017. Lecture Notes in Mechanical Engineering. Springer, Cham.

Sun, H.; Ma, C.; Kim, E.S.; Nowakowsky, G.; Mauer, E.; Bernitsas, M.M. Hydrokinetic energy conversion by two rough tandem-cylinders in flow induced motions: Effect of spacing and stiffness. Renewable Energy, Elsevier BV, v. 107, p. 61-80, jul 2017.

RESPONSIBILITY NOTICE

The author(s) is (are) the only responsible for the printed material included in this paper.